CORROSION SCIENCE AND TECHNOLOGY, Vol.9, No.6(2010), pp.239~246

Numerical Simulation of an Impinging Jet with Various Nozzle-to-strip Distances in the Air-knife System

Hongyun So†, Hyun Gi Yoon[1], and Myung Kyoon Chung

Department of Mechanical Engineering, KAIST, 373-1 Guseong-dong, Yuseong-gu, Deajeon 305-701, Republic of Korea
[1]Korea Atomic Energy Research Institute (KAERI), Daejeon, Republic of Korea
(Received August 5, 2009; Revised December 13, 2010; Accepted December 13, 2010)

When galvanized steel strip is produced through a continuous hot-dip galvanizing process, the thickness of the adhered zinc film is controlled by impinging a thin plane nitrogen gas jet. The thickness of the zinc film is generally affected by impinging pressure distribution, its gradient and shearing stress at the steel strip. These factors are influenced by static pressure of gas spraying at air knife nozzle, a nozzle-to-strip distance and strip and a geometric shape of the air knife, as well. At industries, galvanized steel strip is produced by changing static pressure of gas and a distance between the air knife nozzle and strip based on experimental values but remaining a geometric shape of nozzle. Splashing and check-mark strain can generally occur when a distance between the air knife nozzle and strip is too short, while ability of zinc removal can lower due to pressure loss of impinging jet when a distance between the air knife nozzle and strip is too long. In present study, buckling of the jet and change of static pressure are observed by analyzing flow characteristics of the impinging jet. The distance from the nozzle exit to the strip varies from 6 mm to 16 mm by an increment of 2 mm. Moreover, final coating thickness with change of a distance between the air knife nozzle and strip is compared with each case. An ability of zinc removal with the various distances is predicted by numerically calculating the final coating thickness.

Keywords *: air-knife, check-mark stain, coating thickness, impinging jet, zinc removal area*

1. Introduction

Galvanized steel strip is produced by a continuous hot dip galvanizing process. A heat-treated steel strip is passed through a molten zinc bath and is drawn up with the molten zinc adhered on both strip surfaces. Usually since the thickness of the adhered zinc film is about 10 times thicker than desired thickness, the steel strip is vertically drawn up between a pair of two-dimensional opposing plane gas jets to remove the excessive zinc. In this way the unnecessary molten zinc is wiped down by the impinging gas jets. This wiping mechanism has been well investigated theoretically and experimentally.[1)-3)] The nozzle of the nitrogen gas jet is called the air knife system and this manufacturing method is called the gas wiping process.

In a continuous hot-dip galvanizing process, there are following problems by changing the distance between an air knife and strip. When the distance is too short, the splashing that causes abnormal zinc removal at strip surface appears due to strong impinging pressure.[4)] However, when the distance is increased to suppress the splashing, check-mark strain at the surface is occurred due to buckling of jet and the ability of zinc removal decrease due to the pressure loss of impinging jet. The objective of the present study is to clarify the flow phenomenon changed by the distance between the air knife nozzle and strip by using the large eddy simulation (LES) to analyze the unsteady flow structure which is appeared when the 2-dimensional plane jet impinges against vertical plane. In order to understand the phenomenon based on the fluid dynamic point of view, the 3-D unsteady compressible flow is studied numerically by using the LES turbulence model. Smagorinsky-Lilly SGS is used as the LES sub-gird scale.[5)] In the present study, the changes of pressure, velocity and vortex field for the distance between the air knife and strip are observed through numerical analysis and the splashing and check-mark strain phenomenon are explained and finally, the last coating thickness is predicted.

† Corresponding author: hyso@kaist.ac.kr

2. Numerical analysis

Since the Mach number of the plane impinging jet is around 0.3~0.8 in the gas wiping process, the unsteady 3-D compressible turbulent flow is numerically simulated by using the commercial code, FLUELT to observe the characteristics of the flow field. Computational domain and boundary conditions of the gas wiping system are shown in Fig. 1. It is assumed that there is no vibration by impinging jet and the flow field is homogenous in the span wise direction, and so the symmetric condition is given at both sides of the calculation domain. The length in the z-direction is 100 mm which is one-tenth of the steel strip used in the zinc coating industry. The opposing jet region in the outside of the strip edge is not considered because impinging jet is calculated in the interior region.

The steel strip moves from bottom to top, and the calculation domain in the vertical direction is 60 mm. The atmospheric pressure condition is used at the top and bottom boundaries. The symbols L and d in Fig. 1 represent the distance between the air knife nozzle and strip and slit height of the air knife nozzle, respectively. Cases used in present study are listed in Table 1. The case which distance between the air knife nozzle and strip is 6mm is determined as a basis Case 1. The inside static pressure(P_0) and temperature(T_0) of the air knife are given with 25 kPa(gauge) and 340 K under which the check-mark strain appears in the gas wiping process by the actual air knife, Case 3. The nitrogen gas is used also as working fluid to follow the actual process. The surface of the steel strip is treated as a wall moving at a constant speed of 2.5 m/s in positive y-direction at x=0.

LES technique is used to produce the turbulent flow of the impinging jet. Time step of the unsteady solver

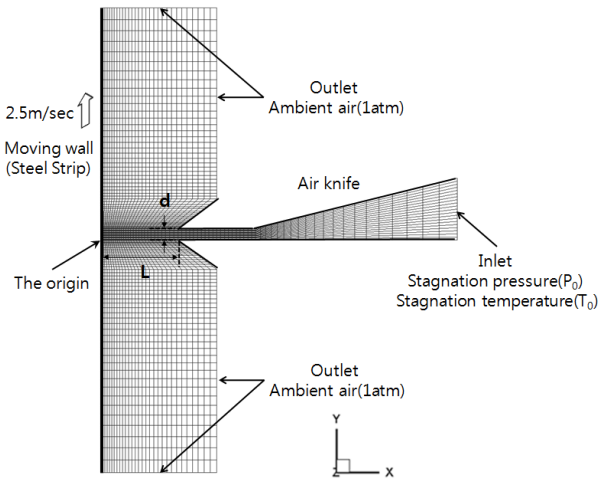

Fig. 1. Computational domain and boundary conditions.

Table 1. Calculation conditions

Case	d [mm]	L [mm]
1	1.5	6
2	1.5	8
3	1.5	10
4	1.5	12
5	1.5	14
6	1.5	16

was fixed to be $\Delta t = 5.0 \times 10^{-7}$ sec which was determined from the smallest grid size and the exit velocity of the plane jet. When the exit velocity is 230 m/sec, the Courant number $N_{courant} = U\Delta t / \Delta x$ is 1.15 for the smallest grid size and it was found that the Courant number varies from about 0.5 to 1.5 in the whole computation domain in the present study. Considering that the appropriate range of the Courant number is generally from 0.3 to 2 in LES simulation, the grid size and time step used in the present study are suitable.[5)-6)] The PISO algorism was used as a pressure-velocity coupling, and bounded central differencing method was applied as a dispersion method which is appropriate for LES technique.

3. Description of the 3-D unsteady flow field of impinging jet

Simulation result of the pressure distribution of impinging jet and steel strip with various nozzle-to-strip distances will be explained in the first place. Fig. 2-(a) shows the pressure contours of the nitrogen gas flow on the xy-plane at the middle of the z-direction (z = 50 mm). Stagnation pressure distribution at the strip is shown in Fig. 3. This follows well the Gaussian distribution clarified by early studies.[7)-8)] As seen Fig. 3, the maximum pressure at the strip of Case 1 and 2 which distance from the exit of the air knife to strip are 6 mm and 8 mm respectively is nearly the same as their static pressure at the air knife. This means that the closer the distance between the air knife and strip becomes, the lower the loss of static pressure becomes. On the other hand, the longer the distance between the air knife and strip becomes, the more increase the loss of static pressure becomes and the wider the range of the impinging region becomes. Furthermore, Fig. 2-(a) shows that high and low static pressure is formed periodically at upper and lower part of jet by the buckling. While the buckling is less generated at Case 1 and 2 because of relatively short distance between the air knife nozzle and strip, Case 3 and 4 have fully developed buckling and Case 5 and 6 have complicated flow field due to the

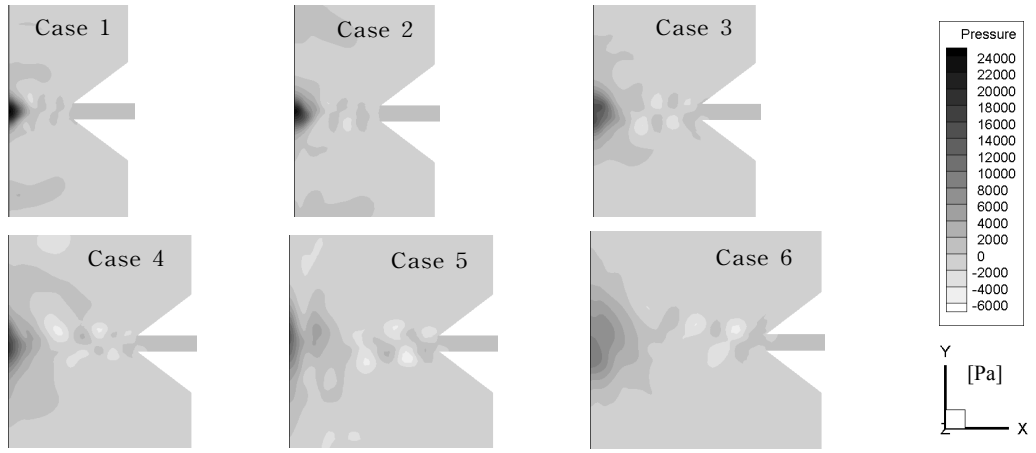

(a) Static pressure contours on xy-plane at z = 50 mm

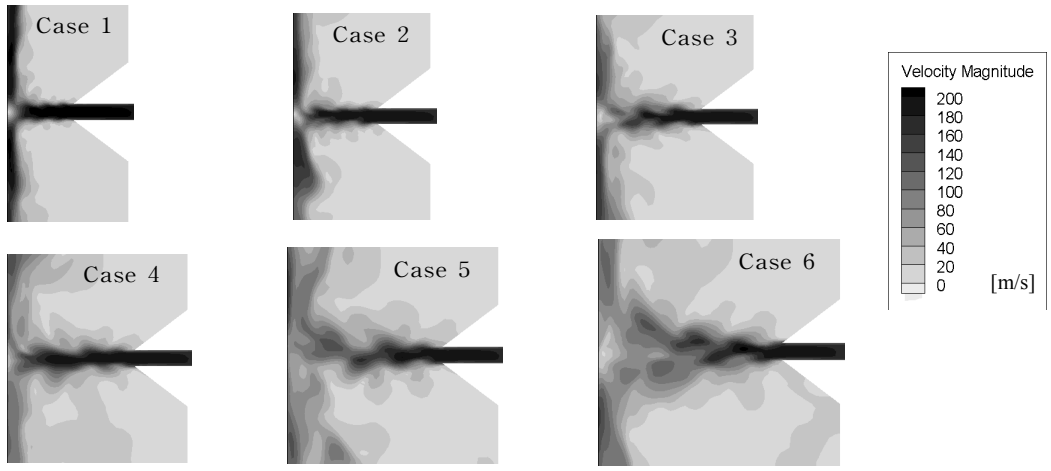

(b) Velocity magnitude contours on xy-plane at z = 50 mm

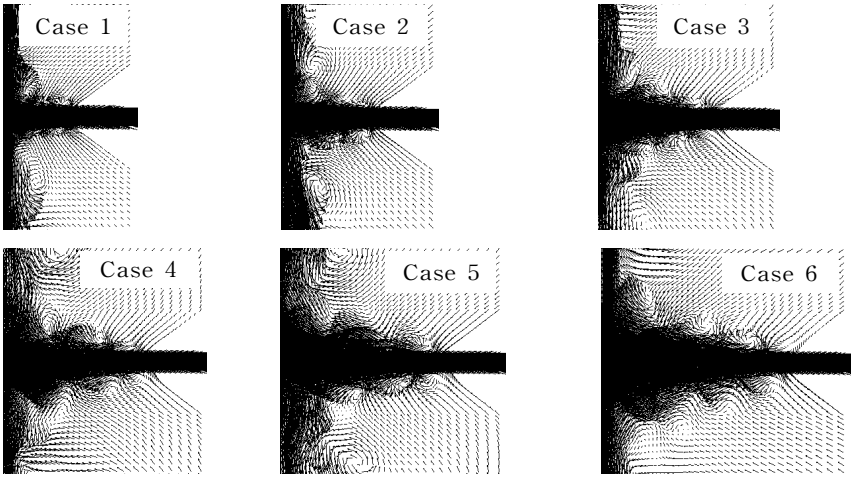

(c) Vortex pairs in the upper and lower part of the jet

Fig. 2. Simulation results for each case.

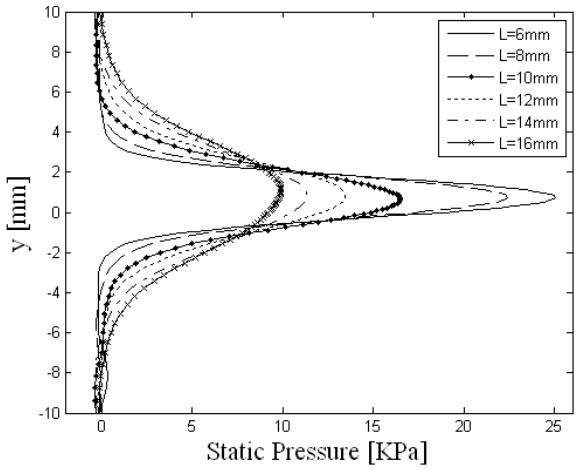

Fig. 3. Static pressure distributions on the strip surface.

entrainment of surrounding air and diffusion of jet. However, the longer the distance between the air knife nozzle and strip becomes, the more increase the static pressure at the surface in range of 2.25 mm≤y≤8 mm. This means that although the maximum static pressure which affects at the strip is decreased as increasing the distance between the air knife nozzle and strip, the static pressure at specific lower and upper region at which the maximum static pressure is operated is relatively high. Therefore, the zinc removal area is wide at there.

Jet impingement region can be divided into two region; inner and outer impinging regions. Inner impinging region is where the gas jet collides on the strip surface nearly normally. Outer impinging region is where the outer part of the jet that diffused slightly in y-direction collides on the strip surface obliquely. Fig. 2-(b) shows the velocity contours of the nitrogen gas flow on the xy-plane at the middle of the z-direction (z = 50 mm). While buckling does not occur at Case 1 and 2 because potential core is not fully developed due to relatively short distance from nozzle exit to strip, buckling of the potential core is observed at Case 3, 4, 5 and 6. However, despite Case 4, 5 and 6 have a short length of potential core, buckling does not definitely occur than Case 3. This reason is that strength of a pair of vortex formed at upper and lower part of the center of impinging jet is largest at Case 3 as shown in Fig. 2-(c).

Fig. 4 shows the static pressure contours on the xz-plane at the y=1.4 mm. As can be seen at Case 3 in Fig. 4, the pressure of the jet deceases periodically along the transverse direction after spraying from the air knife nozzle. As a result of this, center axis of the jet is buckled and distribution of static pressure is changed from 5 kPa to 16 kPa. The closer the distance between the air knife nozzle and strip becomes, the more stable the static pressure at the air knife nozzle is. Also, the longer the distance between the air knife nozzle and strip becomes, the more irregular the static pressure becomes and periodical contours of static pressure does not appear anymore. In order to closely investigate the flow characteristics of the nitrogen gas in the inner impinging region, static pressure contours are displayed on the yz-plane at x = 0.1 mm in Fig. 5.

As can be seen at Case 3 in Fig. 5, the high and low pressure points on the steel strip are appeared repeatedly. It is evident that more molten zinc is removed at the high pressure point in comparison with the low pressure point. Therefore, the zinc coated steel strip would have a wavy strain called check-mark strain. When the distance between the air knife nozzle and strip is short, high and low pressure points are disappeared and nearly uniform pressure is appeared along z-direction of strip because the loss of the static pressure is decreased. On the other hand, when the distance between the air knife nozzle and strip becomes long as can be seen at Case 5 and 6, static pressure which range is about from 10 kPa to 12 kPa widely spreads along z-direction. Since there is no repeatedly pressure points anymore, check-mark strain at the surface would less appear. The final coating thickness, however, is thicker than that from Case 3 due to deterioration of ability of zinc removal.

3.1 Prediction of coating thickness

The coating thickness of the liquid film on the surface of the strip is controlled by the impinging pressure and the shearing stress of the jet flowing along the strip. The liquid film flow is numerically analyzed under assumptions, the liquid flow on the strip is a steady laminar flow, the surface tension of the liquid film is negligible and no-slip condition is applied between the liquid film and strip.[9] The pressure in the liquid film becomes the function of only y with the assumption that the pressure is equal to the pressure on the surface of the liquid film. Therefore, velocity profile is obtained as shown in Eq. (1) by integrating Navier-stokes equation with boundary conditions.

$$v(x,y) = V_s + \frac{1}{\mu}\left[\tau_w x + \left(\frac{dp}{dy} + \rho g\right)\left(\frac{1}{2}x^2 - h(y)x\right)\right] \quad (1)$$

The volumetric liquid flow rate per unit width, q, is calculated by integrating Eq. (1).

$$q = \int_0^{h(y)} v(x,y)dx = V_s h(y) + \frac{1}{2}\frac{\tau_w}{\mu}h(y)^2 - \frac{h(y)^3}{3\mu}\left(\rho g + \frac{dp}{dy}\right) \quad (2)$$

Equation (2) is expressed with the normalized variables

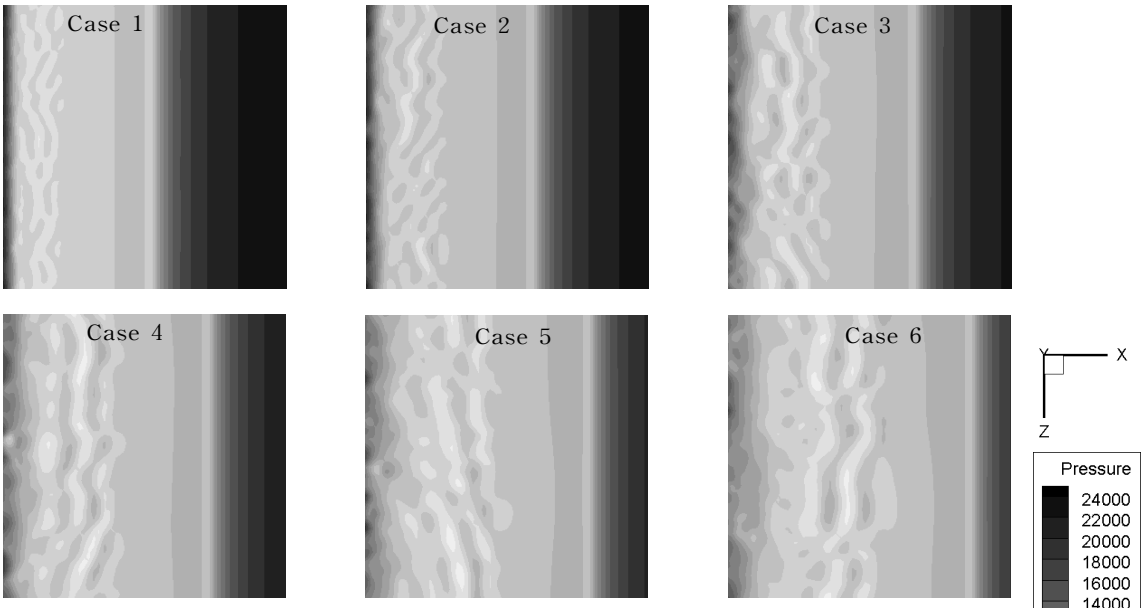

Fig. 4. Static pressure contours on xz-plane at y = 1.4 mm

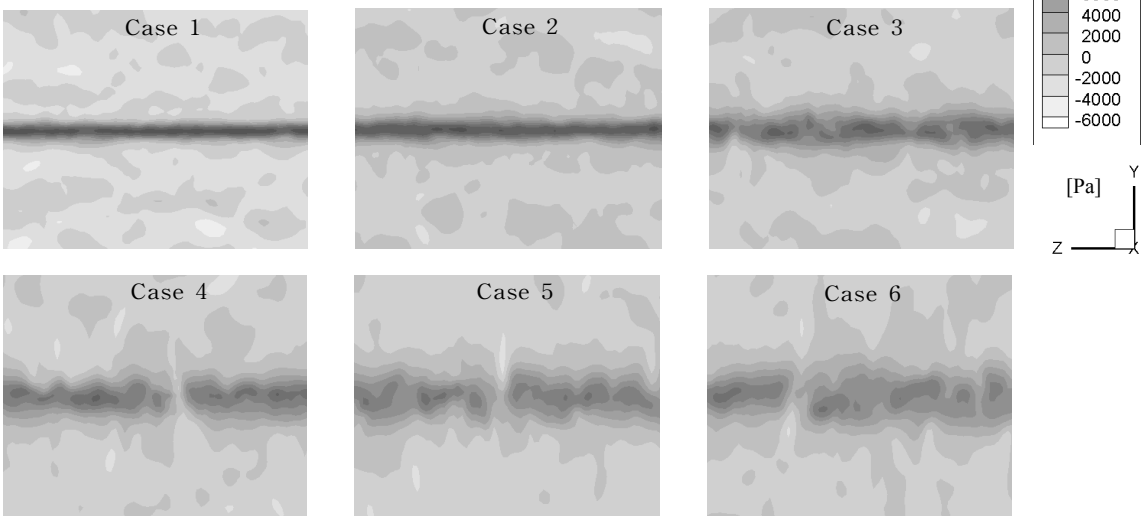

Fig. 5. Static pressure contours in the stagnation line.

and dimensionless physical group as follows:

$$(1+\nabla\hat{P})\hat{h}^3 - 1.5\hat{T}\hat{h}^2 - 3\hat{h} + 2Q = 0 \quad (3)$$

The normalized variables and dimensionless physical group in Eq. (3) are defined as follows:

$$h_0 = \sqrt{\frac{\mu_l V_s}{\rho_l g}} \quad \hat{h} = \frac{h}{h_0} \quad X = \frac{x}{d} \quad Q = \frac{q}{q_0} \quad q_0 = \frac{2}{3} V_s h_0$$

$$\nabla\hat{P} = \frac{\nabla p}{\rho_l g} \quad \hat{T} = \frac{\tau_w}{\tau_0} \quad \tau_0 = \sqrt{\mu_l V_s \rho_l g} \quad (4)$$

Nomenclature

- d Nozzle slot height, m
- g Acceleration of gravity, m/s^2
- h Coating thickness, m
- p Impinging pressure, Pa
- $\nabla\hat{P}$ Dimensionless pressure gradient in y-direction
- q Volumetric liquid flow rate per unit width of strip, m^2/s

$\hat{T}$ Dimensionless shear stress
v Liquid velocity in y-direction, m/s
V_s Moving velocity of the steel strip, m/s
x Distance of horizontal direction, m
y Distance of vertical direction, m

Greek symbols

τ_w Wall shear stress, Pa
μ Dynamic viscosity of liquid zinc, Pa·s
ρ Density of liquid zinc, kg/m^3

Subscript 0 refers to the dragged film flow without wiping and 1 to the liquid phase. The solution of Eq. (3) for determining the film thickness along the longitudinal (vertical) direction $h(y)$ is obtained by solving locally the cubic equation and using the pressure gradient and shear stress distribution obtained by numerical simulation or measurement of an impinging jet on the surface.

Fig. 6 and Fig. 7 show the distribution of shearing stress and the gradient of impinging pressure on the steel strip for each case, respectively. Fig. 8 shows the result of calculated coating thickness for each case by applying the pressure gradient and shear stress into Eq. (3). The values of the coating thickness are shown in Table 2. As a result of numerical analysis, the coating thickness is proportional to the distance between the air knife nozzle and steel strip. Also, the coating thickness has a minimum value at not the center of jet (y = 0) but the upper part of it and then becomes a little thick again. The reason of this is that the shear stress and impinging pressure have a maximum values at the upper part of the center of impingement region as can be seen in Fig. 6 and Fig. 3, respectively.

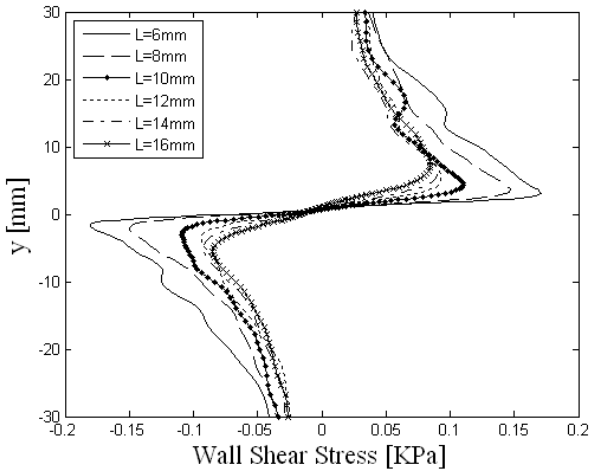

Fig. 6. Shear stress distributions on the strip surface.

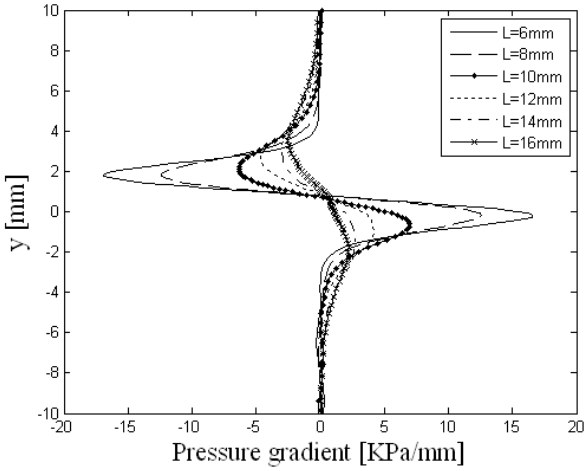

Fig. 7. Pressure gradient distributions on the strip surface.

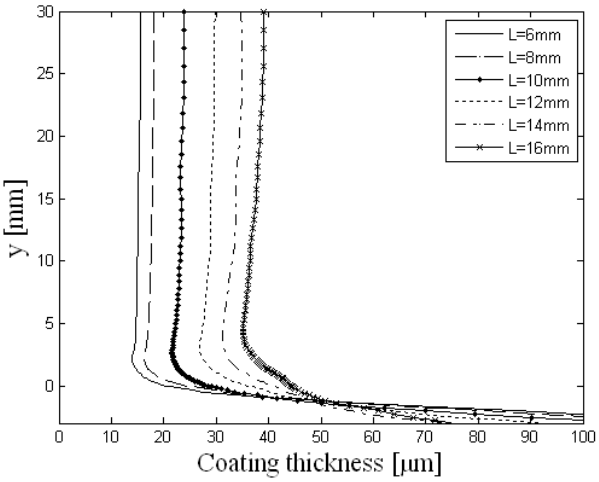

Fig. 8. Comparison of final coating thickness.

The y coordinates on the strip at which the maximum static pressure are appeared are shown in Table. 2 for each case, as well. Since the shear stress becomes lower and gravity effect becomes large at upper part of these points, the coating thickness becomes thick again.

3.2 Zinc removal area

The standard deviations of the maximum pressure along the z-direction for each case are shown in Table. 2. As increasing the standard deviation, the change of the maximum pressure on the strip is changed irregularly. This means that zinc on the strip is removed unstably. The Case 3 which conditions cause appearance of a check-mark strain on the surface in the actual process has relatively high standard deviation of the maximum pressure than other cases. Although Case 6 has a high standard deviation for the maximum pressure, the check-mark strain on the

Table 2. Results of numerical analysis

Case	Coating Thickness [μm]	Max. Pressure [KPa]	Y coordinate of Max. Pressure [mm]	STDEV of Max. Pressure	STDEV of Effective Pressure
1	15.64	24.98	0.750	0.1809	0.2219
2	18.20	22.43	0.750	0.1809	0.2220
3	23.85	16.50	0.675	0.1960	0.3556
4	29.76	13.47	0.825	0.1796	0.2566
5	34.76	11.32	0.900	0.1910	0.3014
6	39.09	9.93	1.125	0.2848	0.1960

Table 3. Comparison of effective impinging area

Case	Effective Impinging Area [mm]
1	0.100
2	0.150
3	0.225
4	0.300
5	0.375
6	0.450

surface is less appeared than Case 3 because the static pressure which could effectively remove zinc is uniformly distributed at the lower and upper part of the maximum static pressure applied points. Because of this the zinc not removed at the impingement point could be taken away as moving the steel strip in positive y-direction. Therefore, although Case 6 could not perfectly remove zinc at jet-plane impinging points, Case 6 has stability for removing zinc because the zinc could remove once more at lower part. In the present study, the pressure having 98 percent strength of the maximum static pressure is assumed as effective pressure, and the standard deviation from maximum static pressure to effective pressure is listed in Table. 2. The standard deviation of the effective pressure for Case 6 is relatively smaller than the others. Therefore, the zinc removal area (or effective impinging area) per unit wide length of steel strip can be defined as follows:

Effective impinging area =
(y-coordinates at which max. static pressure is appeared)-
(y-coordinates at which effective pressure is applied) (5)

Table 3 shows the effective impinging area for each case. Since the effective impinging area of Case 6 is widest, Case 6 would remove zinc through spacious region and suppress the splashing caused by difference between surface tension of zinc film and force on the surface by the impinging pressure.

4. Conclusions

In order to investigate the flow field as changing the distance between the air knife nozzle and steel strip in a continuous hot-dip galvanizing process, the 3-D flow field around the air knife and the moving steel strip is calculated by using the commercial code, FLUENT. Also, LES technique was used to simulate as exactly as possible the unstable and complex 3-D flow field.

As a result of our simulation, it was observed that the coating thickness becomes thin as closing the distance between the air knife nozzle and steel strip, but the splashing would occur because of periodically sudden drop of the static pressure on the surface. On the other hand, although the coating thickness becomes thick as longing the distance from the air knife nozzle to steel strip, the effective impinging area (zinc removal are) is extended because the pressure has a slow gradient and the standard deviation around the maximum static pressure has low value. The check-mark strain on the steel surface at Case 3 would appear severely than other cases because the high and low static pressure along the stagnation line is appeared frequently and the standard deviation of maximum static pressure is largest than others.

Through the present study, 3-D flow field established by impinging a two-dimensional plan jet normally onto a moving steel strip in a relatively short distance is investigated in detail and the flow characteristics as changing the distance between the air knife nozzle and steel strip are clarified by the results of numerical analysis.

References

1. J. M. Buchlin, M. Manna, M. Arnalsteen, M. L. Riethmuller, and M. Dubois, *European Coating Symposium on the Mechanism of Thin Film Coating*, p. 168, World Scientific, Singapore (1996).
2. J. A. Thornton and H. F. Graff, *Metall. Mater. Trans.*

B, **7B**, 607 (1976).
3. Y. Takeishi, A. Yamauchi, and S. Miyauchi, *Tetsu-to-Hagane*, **80**, 37 (1995).
4. C. V. Tu and D. H. Wood, *Exp. Therm. Fluid Sci*., **13**, 364 (1996).
5. H. K. Versteeg and W. Malalasekera, Computational Fluid Dynamics, p. 98, Pearson Prentice Hall, London, 2007.
6. J. H. Ferziger and M. Peric, Computational Methods for Fluid Dynamics, Springer, p. 143, Berlin, 2002.
7. J. J. Schauer and R. H. Eustis, *Tech. Report 3, Dept. Mech. Eng., Stanford Univ*., (1963).
8. S. Beltaos, ASCE J. Hydraulic Div., 102, 1177 (1972).
9. A. Katsuya and O. Tsuyoshi, *7th Int. Conf. on Zinc and Zinc Alloy Coated Steel Sheet*, p. 177, ISIJ, Tokyo, (2007).